2014-05

Statistical Properties of Exciton Fine Structure Splitting and Polarization Angles in Quantum Dot Ensembles

UTD AUTHOR(S): Ming Gong and Chuanwei Zhang

Statistical properties of exciton fine structure splitting and polarization angles in quantum dot ensembles

Ming Gong,[1,2,*] B. Hofer,[3] E. Zallo,[3] R. Trotta,[3,4,†] Jun-Wei Luo,[5,6,‡] O. G. Schmidt,[3] and Chuanwei Zhang[2]

[1]*Department of Physics, The Chinese University of Hong Kong, Shatin, New Territories, Hong Kong, China*

[2]*Department of Physics, The University of Texas at Dallas, Richardson, Texas 75080, USA*

[3]*Institute for Integrative Nanosciences, IFW Dresden, Helmholtzstr. 20, D-01069 Dresden, Germany*

[4]*Institute of Semiconductor and Solid State Physics, Johannes Kepler University Linz, Altenbergerstr. 69, A-4040 Linz, Austria*

[5]*State Key Laboratory of Superlattices and Microstructures, Institute of Semiconductors, Chinese Academy of Sciences, P.O. Box 912, Beijing 100083, China*

[6]*Synergetic Innovation Center of Quantum Information and Quantum Physics, University of Science and Technology of China, Hefei, Anhui 230026, China*

(Received 26 June 2013; revised manuscript received 1 November 2013; published 20 May 2014)

We develop an effective model to describe the statistical properties of exciton fine structure splitting (FSS) and polarization angle in quantum dot ensembles (QDEs) using only a few symmetry-related parameters. The connection between the effective model and the random matrix theory is established. Such effective model is verified both theoretically and experimentally using several rather different types of QDEs, each of which contains hundreds to thousands of QDs. The model naturally addresses three fundamental issues regarding the FSS and polarization angels of QDEs, which are frequently encountered in both theories and experiments. The answers to these fundamental questions yield an approach to characterize the optical properties of QDEs. Potential applications of the effective model are also discussed.

DOI: 10.1103/PhysRevB.89.205312 PACS number(s): 78.67.Hc, 42.50.−p, 73.21.La, 81.07.Ta

I. INTRODUCTION

The fine structure splitting (FSS) of excitons in self-assembled quantum dots (QDs) poses a major obstacle for the realization of entangled photon pairs, thus has been a subject of extensive investigations in the past decade [1–11]. Nowadays, it is known that FSS arises from the intrinsic nonequivalence between [110] and [1$\bar{1}$0] directions in zinc-blende crystals, which reduces the symmetry of the underlying lattice from T_d to C_{2v} for lens-shaped QDs. Such nonequivalence is enhanced by lattice mismatch induced local strain and dot shape. Shape irregularities, alloys, and interface effects [12,13] can further reduce the symmetry to C_1 [14]. A single field (e.g., electric field [15–20], magnetic field [2,21], or anisotropic stress [14,22–26]) alone is not sufficient to eliminate FSS, and two nonequivalent fields have to be combined [8,9]. Generally, FSS depends strongly on the local details of QDs. For instance, two QDs with identical morphology but tiny difference in alloy atomistic arrangement may have fairly different FSS and polarization angle [10]. Therefore, we confront three fundamental questions that are hard to understand: (i) Why is the probability of finding QDs with vanishing FSS in general very small? (ii) Why do FSS and polarization angle differ dramatically from QD to QD? (iii) Is there any direct connection between FSS, polarization angle, and morphology of QDs? The understanding of these issues is also important for the applications of QDEs in QD lasers [27–31], where realization of good uniformity in optical emission requires the answers to the above questions.

In this work, we address these fundamental issues by developing an effective model to describe the statistics of FSS and polarization angle for QDEs from symmetry argument. We show that their statistics can be fully characterized using only a few symmetry-related parameters. The connection of this model to random matrix theory is also established. This effective model is verified both theoretically and experimentally using several rather different types of QDEs, each of which contains hundreds to thousands of QDs. Potential applications of the effective model are also discussed. These results yield an approach to characterize the optical properties of QDEs.

II. THEORETICAL MODEL

From the symmetry viewpoint, the Hamiltonian for a single QD can be written as $H = H_{2v} + V_1$, where H_{2v} contains the kinetic energy and the potential with C_{2v} symmetry, and V_1 is the perturbation potential with C_1 symmetry. The eigenvectors of H_{2v} can be written as $|3\rangle = |\Gamma_2 + i\Gamma_4\rangle$ and $|4\rangle = |\Gamma_2 - i\Gamma_4\rangle$, where the standard basis functions for Γ_2 and Γ_4 are x and y, respectively [32]. So, we see that these two wave functions are exactly along either the [110] or [1$\bar{1}$0] direction. This basic feature is ensured by C_{2v} symmetry. On the other hand, the time-reversal operator Θ for an exciton is a direct product of time-reversal operators for both an electron and hole, hence $\Theta^2 = 1$. Moreover, all the eigenvalues of exciton in QD are nondegenerate. Thus, we can prove exactly that the wave functions of $|3\rangle$ and $|4\rangle$ have real representation. This basic feature is ensured by time-reversal symmetry. For these reasons, the Hamiltonian H can be written as [14]

$$H = \bar{E} + \delta\sigma_z + \kappa\sigma_x, \tag{1}$$

where $\bar{E} + \delta = \langle 3|H|3\rangle$, $\bar{E} - \delta = \langle 4|H|4\rangle$, $\kappa = \langle 3|V_1|4\rangle$, and δ, $\kappa \in \mathbb{R}$. σ_x and σ_z are Pauli matrices. $\bar{E}$ is the exciton energy and $\Delta = 2\sqrt{\kappa^2 + \delta^2}$ is the FSS. κ describes the

*skylark.gong@gmail.com
†rinaldo.trotta@jku.at
‡jwluo@semi.ac.cn

coupling between two bright states, leading to the deviation of the emission lines from the [110] and [1$\bar{1}$0] directions. The wave function of the bright exciton can be written as $\psi = \cos(\theta)|3\rangle + \sin(\theta)|4\rangle$, where θ is the polarization angle with $\tan(\theta) = \kappa^{-1}(\kappa \pm \sqrt{\delta^2 + \kappa^2})$. Hence,

$$\delta = \pm\frac{\Delta}{2}\sin(2\theta), \quad \kappa = \mp\frac{\Delta}{2}\cos(2\theta). \tag{2}$$

The V_1 Hamiltonian perturbation term can be uniquely determined with the following recipe. Assume V is the total potential of a single QD (including all types of interactions), and G contains all irreducible representations of the C_{2v} group. For any $g \in G$, $gH_{2v}g^{-1} = H_{2v}$, therefore

$$H_{2v} = T + \left(\sum_{g\in G} gV(\mathbf{r})g^{-1}\right) \Big/ |G|, \tag{3}$$

where T is the kinetic energy and $|G|$ is the number of symmetry operators. Then,

$$V_1(\mathbf{r}) = V(\mathbf{r}) - \left(\sum_{g\in G} gV(\mathbf{r})g^{-1}\right) \Big/ |G|. \tag{4}$$

Obviously, $\sum_g gV_1(\mathbf{r})g^{-1} \equiv 0$ for any $\mathbf{r}$. The C_{2v} symmetry ensures the direct connection between $\mathbf{r}$ and $g\mathbf{r}g^{-1}$, whereas there is no correlation for other coordinate pair ($\mathbf{r}$, $\mathbf{r}'$) when $\mathbf{r}' \neq g\mathbf{r}g^{-1}$. Therefore, V_1, which depends essentially on the local morphology details of QD, should change rapidly in real space in both sign and magnitude. We need to emphasize that the result in Eq. (4) is quite general, for which reason the basic observations in this work for QDEs with C_{2v} symmetry can be easily extended to other symmetries (see discussion in Sec. IV).

The major difference between a single QD and a QDE is that in the latter case, the morphology variations of different QDs lead to the variations of both H_{2v} and V_1 in a QDE. To make the physical picture more transparently, we rewrite $H_{2v} = \bar{H}_{2v} + \delta H_{2v}$, where $\bar{H}_{2v} = \langle H_{2v}\rangle$ is an ensemble-averaged Hamiltonian and δH_{2v} denotes the variation from QD to QD. V_1 can be treated as a random potential from the viewpoint of QDEs due to its peculiar feature in Eq. (4). The δH_{2v}, although lacking a similar feature, also possesses some degrees of randomness. Although the effective model in Eq. (1) for a single QD is still valid for describing the properties of QDEs, δ and κ should be treated as independent random numbers satisfying some particular distributions. Note that both δH_{2v} and V_1 contribute to the randomness of δ, but only V_1 contributes to the randomness of κ. In this sense, we expect $\langle\kappa\rangle = 0$, but $\langle\delta\rangle \neq 0$ because QDs with C_{2v} symmetry ($V_1 \equiv 0$) still have finite FSS. Hereafter, we define $\delta = \delta_0 + \delta'$, where $\delta_0 = \langle\delta\rangle$ directly characterizes the shape anisotropy effect of the QDEs (see following).

It is expected intuitively that the distributions of FSS (Δ) and polarization angle (θ) in a QDE should strongly depend on morphological details of each QD, including sizes (base diameters, heights), shapes, alloy profiles, etc. However, it is impossible to precisely determine all these parameters for all QDs in practical experiments [33–35]. We can circumvent this difficulty by using several symmetry-related parameters to fully characterize the statistics of Δ and θ in QDEs. In general, the distribution of any observable quantity, saying $f = f(\kappa,\delta_0,\delta')$, is defined as

$$P(z) = \int d\delta' d\kappa\, \delta(f - z)\mathcal{N}(\delta',\sigma_\delta)\mathcal{N}(\kappa,\sigma_\kappa), \tag{5}$$

where κ and δ' satisfy normal distributions $\mathcal{N}(x,\sigma)$, with variations $\sigma_\kappa^2 = \langle\kappa^2\rangle$ and $\sigma_\delta^2 = \langle\delta'^2\rangle$, respectively. The exact distribution functions for Δ and θ can be found in the Supplemental Material [36]. This strategy enables us to understand and then engineer the statistics of FSS and polarization angle of QDEs without knowing the morphological details of each individual QD. From the statistical viewpoint, the morphological details only affect the magnitude of the parameters $(\delta_0,\sigma_\kappa,\sigma_\delta)$.

The result is particularly interesting when QDs in the ensemble have rotational symmetry [37], i.e., two bright states are degenerate ($\delta_0 = 0$) and the basis can be chosen along any two orthogonal directions. In this case, $\sigma_\delta = \sigma_\kappa$, and the distribution of FSS Δ is found to be [37]

$$P(s) = \frac{\pi}{2}s\exp\left(-\frac{\pi}{4}s^2\right), \tag{6}$$

where $s = \Delta/\langle\Delta\rangle$. This is the standard level-spacing distribution of the Gaussian orthogonal ensemble in random matrix theory [37]. In a real QDE without rotational symmetry ($\sigma_\delta \neq \sigma_\kappa$), but $\delta_0 \sim 0$, we find

$$P(\Delta) = \frac{\Delta}{4\sigma_\delta\sigma_\kappa}\exp(-A_+\Delta^2)I_0(A_-\Delta^2), \tag{7}$$

where $A_\pm = 1/(16\sigma_\kappa^2) \pm 1/(16\sigma_\delta^2)$ and $I_0(x)$ is the modified Bessel function of the first kind. These results clearly demonstrate the strong repulsion between levels. More specifically, the independence of off-diagonal and diagonal elements leads to the appearance of the s term in Eq. (6), which leads the possibility of finding QDs with vanishing FSS to be very small. It is in stark contrast to trivial random matrix without off-diagonal elements where strong attraction between levels leads level spacings to be described by Poisson distribution [38] and leads the possibility of finding vanishing FSS to be maximum (see solid line in Fig. 2). This result agrees well with recent experimental measurements, where only rare QDs possess vanishing FSS. We also find that for a large class of QDEs without exact rotational symmetry, their FSS can still be well described by Eq. (6). In this sense, the ideal random matrix model [37] provides a unique angle for understanding the statistics of FSS in QDEs.

The distribution of the polarization angle $\theta \in [-\pi/2,\pi/2]$ reads as [39]

$$P(\theta) = \frac{1}{\pi}\frac{1}{\eta\,\sin^2(2\theta) + \eta^{-1}\cos^2(2\theta)} \tag{8}$$

when $\delta_0 = 0$, where $\eta = \sigma_\delta/\sigma_\kappa$. Apparently, $P(\theta) = 1/\pi$ when $\eta = 1$, and reaches the maximum at $\theta = 0, \pm\pi/2$ when $\eta > 1$, or at $\theta = \pm\pi/4$ when $\eta < 1$. The period of $P(\theta)$ is $\pi/2$. It is worth to emphasize that the fluctuation of θ is induced by the random coupling between the bright states through V_1, therefore it is not an extrinsic effect [40]. In the following, the validity of the above analytical results will be confirmed both theoretically and experimentally using several rather different

types of QDEs; some of these QDEs even have relative large δ_0. In the following, the validity of the above one-parameter equations will also be examined carefully.

In the limit of $\delta_0 \gg \sigma_\delta, \sigma_\kappa$, the distribution of θ becomes very simple and can be understood as follows. The emissions should polarize either along $\theta = 0$ or $\pm\pi/2$, thus $\eta \gg 1$. The FSS is most likely to be observed at $\Delta \sim \delta_0$ in such types of QDEs, and the distribution of FSS, which is close to a Gaussian function with width $\sqrt{\sigma_\delta^2 + \sigma_\kappa^2}$, decays rapidly to zero when $|\Delta - \delta_0| \gg \sigma_\delta$. This limit corresponds to QDEs with strong shape anisotropy.

III. NUMERICAL AND EXPERIMENTAL VERIFICATIONS

The above results are further verified in several rather different types of QDEs by performing large-scale atomistic numerical simulations or experimental measurements. The simulation is based on the well-established pseudopotential method [41–43]. Due to the large lattice mismatch (~7%) between the dot material (InAs) and the matrix (GaAs), we first have to relax the total strain energy to get the true equilibrium positions $\{\mathbf{R}_{i,\alpha}\}$, with i the site index and α the atom type index. Here, the total strain energy is modeled using the valence force field (VFF) model [11,43,44], which has been successfully applied to various III-V group semiconductor systems [8,11,43,45–47]. For this reason, any small variations in alloy configuration in QDs can lead to small variation of equilibrium positions, thus its influence can be captured by our atomistic theory. This small variation can lead to small changes of exciton energies at the order of ~1 meV, but can dramatically change FSSs and polarization angles. The eigenvalues of the exciton are solved based on the linear combination of bulk bands (LCBB) method plus the configuration interaction method (see more details in Refs. [41–43]). In this work, three different $In_xGa_{1-x}As/GaAs$ QDEs are considered: (T1) lens QDs with $x = 0.6$, diameter $D = 25$ nm, height $h = 3.5$ nm; (T2) elongated QDs with $x = 0.6$, diameter along [110] ($[1\bar{1}0]$) direction $D_{[110]} = 26$ nm ($D_{[1\bar{1}0]} = 24$ nm), $h = 3.5$ nm; (T3) lens QDs where x, D, and h are variables, with $\langle x \rangle = 0.6$, $\langle D \rangle = 25$ nm, $\langle h \rangle = 3.5$ nm, and variations up to 10% of the corresponding mean values. In all these simulations, the different alloy configurations are controlled by a random seed, through which we can mimic the random alloy effect in realistic QDEs in experiments.

In experiments, we consider four different QDEs. The samples are grown by solid-source molecular beam epitaxy on the GaAs (001) substrate. GaAs/AlGaAs QDs are obtained by infilling self-assembled nanoholes fabricated *in situ* either by droplet etching [48] or $AsBr_3$ etching [49]. The indium-flushed self-assembled In(Ga)As/GaAs QDs are grown by the Stranski-Krastanov technique [50]. Excitons confined in the GaAs QD (QDE E1), In(Ga)As QD (QDE E4), and GaAs quantum-well potential fluctuations (QDEs E2 and E3, respectively) are investigated. All numerical results show exact linear orthogonality for the two bright states, and in experiments, we do not observe clear evidence for nonorthogonal emissions [51,52] from the microphotoluminescence spectroscopy measurements at low temperature.

TABLE I. Summarized parameters for different QDEs. N is the total number of simulated or measured QDs. E_X (eV) is the mean exciton energy, and σ_X (meV) is the variation of the exciton energies. $\langle\kappa\rangle$, σ_κ, δ_0, σ_δ, $\langle\Delta\rangle$ (the mean value of FSS) are all in units of μeV. η has been defined in Eq. (8). $\mathcal{G}^{(2)} = \langle(\delta - \langle\delta\rangle)(\kappa - \langle\kappa\rangle)\rangle/\sigma_\delta\sigma_\kappa$ measures the cross correlation between two random numbers. $\mathcal{P}$ (%), estimated with Eq. (6), denotes the probability of QDs with FSS smaller than 1 μeV.

QDE	T1	T2	T3	E1	E2	E3	E4
N	1351	1381	7714	204	412	401	240
E_X	1.240	1.210	1.186	1.598	1.722	1.768	1.386
σ_X	2.9	3.0	28.3	2.5	3.6	5.1	4.4
$\langle\kappa\rangle$	−0.1	−0.2	−0.2	−0.1	0.2	−0.3	−0.4
σ_κ	1.7	2.0	1.5	2.1	2.3	1.3	4.4
δ_0	−0.1	−2.9	0.6	15.9	−18.4	−3.5	−1.7
σ_δ	1.4	1.8	1.3	3.0	13.6	10.2	4.8
$\langle\Delta\rangle$	4.0	7.7	3.8	32.6	39.7	15.4	11.7
η	0.88	1.99	1.04	7.80	7.53	5.26	1.0
$\mathcal{G}^{(2)}$	0.002	0.003	~0.0	−0.041	−0.298	0.114	−0.08
$\mathcal{P}$	5.0	1.3	5.7	~0.0	0.2	0.1	0.5

We study several rather different QDEs here to show the validity of the effective model. This general model is derived from purely symmetry argument, thus can be applied to different QDEs. In the following, we choose QDEs T1, T2, E1, and E2 to present our major findings, while all the parameters of the QDEs, including fitted results, are summarized in Table I for comparison. More details can be found in the Ref. [36].

It is readily observed that for all QDEs the distributions of δ and κ [see Figs. 1(a)–1(d)] can be well fitted with Gaussian functions, and these random variables are independent of exciton energies [see Figs. 1(e) and 1(f)]. For QDEs with circular base geometry (T1 and T3), $\delta_0 \sim 0$, whereas in elongated QDE T2 [Fig. 1(b)], the shape anisotropy leads to finite δ_0. These observations qualitatively agree with the results in experiments [see Figs. 1(c) and 1(d)], where QDs are remarkably elongated either along the [110] or $[1\bar{1}0]$ direction. The cross correlation $\mathcal{G}^{(2)}$ between δ and κ s(ee Table I) is generally very small, indicating that these two variables are indeed independent random numbers. The experimental measured correlations are larger than that in the simulations because much fewer numbers of QDs are measured in experiments for each QDE. $\langle\kappa\rangle \sim 0$ is also consistent with the expectation.

The shape anisotropy has a dominant contribution to δ_0, which hence can be used to quantitatively measure the shape anisotropy effect of QDEs. We observe that the anisotropic effect from the lattice nonequivalence of the [110] and $[1\bar{1}0]$ directions in zinc-blende crystal leads to a fairly small δ_0, whereas the anisotropy from shape elongation generally leads to significant δ_0 (hence large FSS), as observed in QDE T2 and E1–E4. In experiments, the QDs exhibit apparent elongation either along the [110] or $[1\bar{1}0]$ direction, and such strong shape anisotropic effect is also expected for the quantum-well potential fluctuation QDEs [22]. In this sense, this conclusion is consistent with the recent reports by Plumhof [22] and Huo [53].

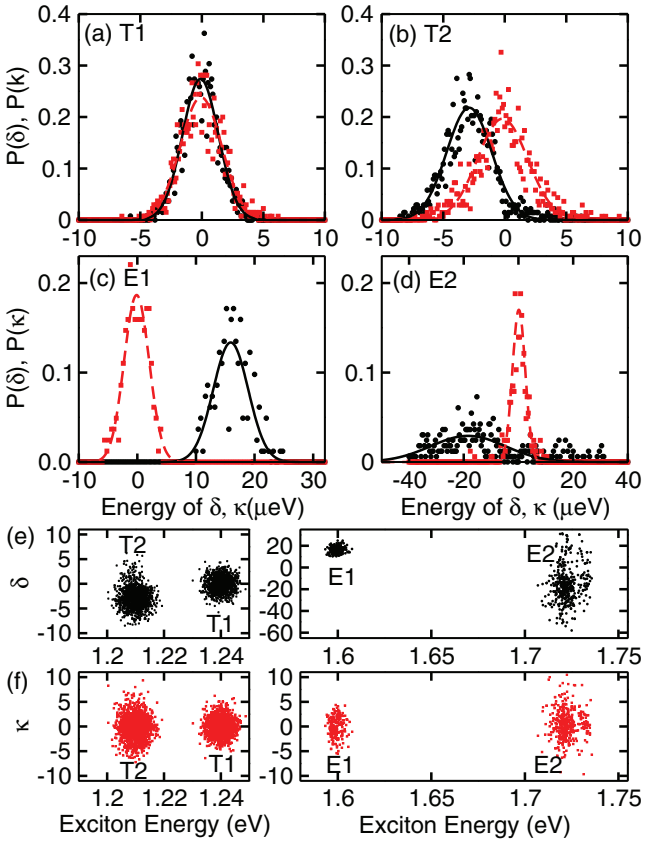

FIG. 1. (Color online) (a)–(d) distributions of δ (•) and κ (■) for several different QDEs. The solid lines and dashed lines are the best fit to Gaussian distribution functions (see Table I). The exciton energy dependence of δ and κ is plotted in (e) and (f), respectively.

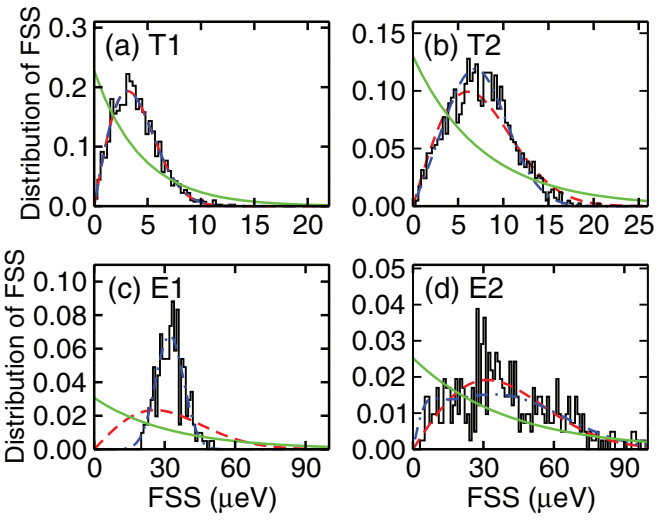

FIG. 2. (Color online) Distributions of FSS for several different QDEs. In each panel, the folded line represents numerical and experimental data, the dashed line is the best fit using Eq. (6), and the dotted-dashed line is from direct calculation using Eq. (5) with the three parameters from Table I. The solid line is the Poisson distribution with the mean FSS equal to $\langle\Delta\rangle$.

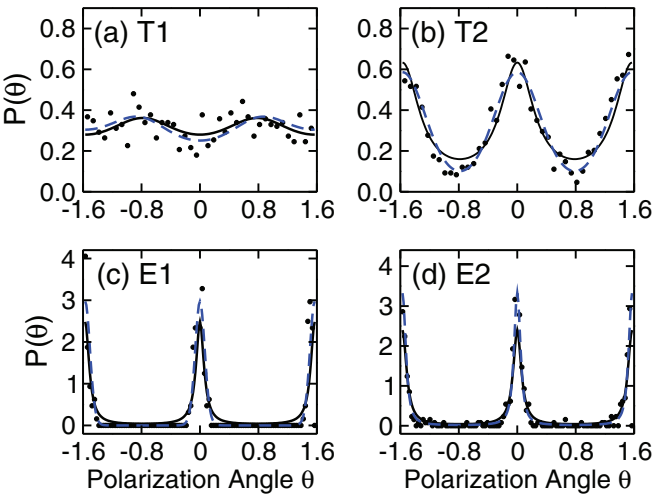

FIG. 3. (Color online) Distributions of polarization angle for several different QDEs. In each panel, the symbols represent the numerical and experimental data, the solid line is the best fit using Eq. (8), and the dashed line is direct calculation using Eq. (5) with the three parameters from Table I.

The distributions of FSS are presented in Fig. 2. The dashed lines are the best fit to Eq. (6), while the dotted-dashed lines are calculated from Eq. (5) with three parameters δ_0, σ_δ, and σ_κ obtained directly by fitting δ and κ to a Gaussian function (see Fig. 1). The excellent agreement between analytic fitting functions and numerical and experimental data for $\delta_0 < 2\sigma_\delta$ showcases that FSS distributions can be well described by a simple model based on random matrix theory, although it is somewhat poorer for QDEs with large δ_0/σ_δ (see QDE E1). The distributions of polarization angles are presented in Fig. 3 and even better agreements than FSS are generally obtained. The good agreement between analytical curves from Eq. (5) and simulations/experiments clearly demonstrates the validity of our effective model. Here, we have also justified the validity of Eqs. (6) and (8) in the limit when $\delta_0 \neq 0$ to providean important basis for future research in QDEs and related semiconductor nanostructures.

IV. APPLICATIONS AND DISCUSSIONS

We now answer the three fundamental questions raised in the Introduction. First, the probability of finding QDs with FSS smaller than homogeneous broadening (1 μeV) reads as

$$\mathcal{P} = \int_0^{1\,\mu\text{eV}} P(\Delta)d\Delta \sim \frac{(1\ \mu\text{eV})^2}{8\sigma_{\delta'}\sigma_\kappa}, \tag{9}$$

where $P(\Delta)$ is defined in Eq. (7) and $\delta_0 = 0$ is assumed. For typical values of σ_δ and σ_κ, $\mathcal{P} \sim 1\%$. When $\delta_0 \neq 0$, a prefactor $\exp(-\delta_0^2/2\sigma_\delta^2)$ arises, which further suppresses $\mathcal{P}$ [see Table I (Q:I)]. Second, with a random potential V_1, it is possible to observe two QDs with the same exciton energies and FSSs, but fairly different polarization angles, therefore in principle no obvious correlation between FSS and polarization angle can be derived (Q:II). Finally, due to the randomness of δ and κ, the morphology effect can be missed out in experiments with a single QD [12,13]. However, it can be recovered from

experiments with QDEs. We show the shape anisotropy has a dominant contribution to δ_0, thus, this value can be used to characterize the shape anisotropy of QDEs. In particular, for a QDE with a large FSS ($\delta_0 \gg \sigma_\delta, \sigma_\kappa$), the FSS itself can be used to characterize the shape anisotropy of the QDE, in which condition the emissions should almost polarize along either the [110] or [1$\bar{1}$0] direction (Q:III).

Several important applications of our model are in order. First, the basic idea can be easily generalized to study the optical properties of high-symmetric QDEs. Although the two bright states are degenerate for QDs with C_{3v} or D_{2d} symmetry [54], the random term V_1 can still render the probability of finding QDs with vanishing FSS small, as shown in recent experiments [55–57]. For high-symmetric QDEs, the rotational symmetry ensures that only one parameter $\sigma_\kappa = \sigma_\delta = \sigma$ is required to fully characterize the statistics of FSS and the polarization angle. In other words, these QDEs are always exact Gaussian orthogonal ensembles. We estimate $\sigma \sim 1$ μeV using the results from Refs. [55,56], which are smaller than that in C_{2v} symmetric QDEs (Table I). As a result, $\mathcal{P}$ can be greatly enhanced [58]. Second, the effective model is derived purely from the symmetry argument, so it is also applicable to study the optical properties of other semiconductor nanostructures, e.g., quantum rod, quantum ring, and colloid nanocrystals [59–61]. As a generic feature, all physical observations should exhibit some degrees of random fluctuations [62]. Third, the leasing from QDEs requires the QDs have good uniformity in optical emissions [27–31]. The distribution of polarization, which is characterized by η, provides important basis in future experiments to improve the uniformity of emissions from QDE. Our results show that QDEs with relative large shape anisotropy are essential for this application. Finally, these results also show that controlling the shape anisotropy (δ_0) of the QDE is essential to increase $\mathcal{P}$ without post treatments, and such controllability has already been demonstrated in recent experiments [63–65]. Contrarily to the third point, the Gaussian orthogonal QDE with $\delta_0 \sim 0$ is best suitable for its application as entangled photon emitters in quantum information science. We hereby conclude that all these results and insights yield a completely general approach to characterize the optical properties of QDEs.

ACKNOWLEDGMENTS

We have the pleasure to thank A. Rastelli in JKU for his valuable discussions, and also for his contribution in creating effective collaboration between different groups. This work is supported by Hong Kong RGC/GRF Projects (No. 401011 and No. 2130352) and the Chinese University of Hong Kong (CUHK) Focused Investments Scheme. B.H., E.Z., R.T., and O.G.S. are partially supported by BMBF QuaHL-Rep (Contract No. 01BQ1032). C.Z is supported by ARO (Grant No. W911NF-12-1-0334, with part of the fund from DARPA-YFA), and NSF-PHY (Grant No. 1104546). J.W.L. is supported by the National Young 1000 Talents Plan.

[1] N. Akopian, N. H. Lindner, E. Poem, Y. Berlatzky, J. Avron, D. Gershoni, B. D. Gerardot, and P. M. Petroff, Phys. Rev. Lett. **96**, 130501 (2006).
[2] R. M. Stevenson, R. J. Young, P. Atkinson, K. Cooper, D. A. Ritchie, and A. J. Shields, Nature (London) **439**, 179 (2006).
[3] R. Hafenbrak, S. M. Ulrich, P. Michler, L. Wang, A. Rastelli, and O. G. Schmidt, New J. Phys. **9**, 315 (2007).
[4] A. J. Hudson, R. M. Stevenson, A. J. Bennett, R. J. Young, C. A. Nicoll, P. Atkinson, K. Cooper, D. A. Ritchie, and A. J. Shields, Phys. Rev. Lett. **99**, 266802 (2007).
[5] R. J. Young, R. M. Stevenson, P. Atkinson, K. Cooper, D. A. Ritchie, and A. J. Shields, New J. Phys. **8**, 29 (2006).
[6] R. J. Young, R. M. Stevenson, A. J. Hudson, C. A. Nicoll, D. A. Ritchie, and A. J. Shields, Phys. Rev. Lett. **102**, 030406 (2009).
[7] L. He, M. Gong, C.-F. Li, G.-C. Guo, and A. Zunger, Phys. Rev. Lett. **101**, 157405 (2008).
[8] J. Wang, M. Gong, G.-C. Guo, and L. He, Appl. Phys. Lett. **101**, 063114 (2012).
[9] R. Trotta, E. Zallo, C. Ortix, P. Atkinson, J. D. Plumhof, J. van den Brink, A. Rastelli, and O. G. Schmidt, Phys. Rev. Lett. **109**, 147401 (2012).
[10] Ranber Singh and Gabriel Bester, Phys. Rev. B **84**, 241402(R) (2011).
[11] Ming Gong, Kaimin Duan, Chuan-Feng Li, Rita Magri, Gustavo A. Narvaez, and Lixin He, Phys. Rev. B **77**, 045326 (2008).
[12] G. Bester, S. Nair, and A. Zunger, Phys. Rev. B **67**, 161306 (2003).
[13] G. Bester and A. Zunger, Phys. Rev. B **71**, 045318 (2005).
[14] M. Gong, W. Zhang, G.-C. Guo, and L. He, Phys. Rev. Lett. **106**, 227401 (2011).
[15] K. Kowalik, O. Krebs, A. Lemaitre, S. Laurent, P. Senellart, P. Voisin, and J. Gaj, Appl. Phys. Lett. **86**, 041907 (2005).
[16] B. D. Gerardot, S. Seidl, P. A. Dalgarno, R. J. Warburton, D. Granados, J. M. Garcia, K. Kowalik, O. Krebs, K. Karrai, A. Badolato, and P. M. Petroff, Appl. Phys. Lett. **90**, 041101 (2007).
[17] M. Vogel, S. Ulrich, R. Hafenbrak, P. Michler, L. Wang, A. Rastelli, and O. Schmidt, Appl. Phys. Lett. **91**, 051904 (2007).
[18] S. Marcet, K. Ohtani, and H. Ohno, Appl. Phys. Lett. **96**, 101117 (2010).
[19] J. W. Luo, R. Singh, A. Zunger, and G. Bester, Phys. Rev. B **86**, 161302 (2012).
[20] A. J. Bennett, M. A. Pooley, R. M. Stevenson, M. B. Ward, R. B. Patel, A. B. de la Giroday, N. Sköld, I. Farrer, C. A. Nicoll, D. A. Ritchie, and A. J. Shields, Nat. Phys. **6**, 947 (2010).
[21] R. M. Stevenson, R. J. Young, P. See, D. G. Gevaux, K. Cooper, P. Atkinson, I. Farrer, D. A. Ritchie, and A. J. Shields, Phys. Rev. B **73**, 033306 (2006).
[22] J. D. Plumhof, V. Krapek, L. Wang, A. Schliwa, D. Bimberg, A. Rastelli, and O. G. Schmidt, Phys. Rev. B **81**, 121309(R) (2010).
[23] R. Singh and G. Bester, Phys. Rev. Lett. **104**, 196803 (2010).
[24] S. Seidl, M. Kroner, A. Hagele, K. Karrai, R. J. Warburton, A. Badolato, and P. M. Petroff, Appl. Phys. Lett. **88**, 203113 (2006).
[25] Christopher E. Kuklewicz, Ralph N. E. Malein, Pierre M. Patroff, and Brian D. Gerardot, Nano Lett. **12**, 3761 (2012).

[26] Luca Sapienza, Ralph N. E. Malein, Christopher E. Kuklewicz, Peter E. Kremer, Kartik Srinivasan, Andrew Griffiths, Edmund Clarke, Ming Gong, Richard J. Warburton, and Brian D. Gerardot, Phys. Rev. B (to be published).

[27] Hideaki Saito, Kenichi Nishi, Shigeo Sugou, and Yoshimasa Sugimoto, Appl. Phys. Lett. **71**, 590 (1997).

[28] P. Jayavel, H. Tanaka, T. Kita, O. Wada, H. Ebe, M. Sugawara, J. Tatebayashi, Y. Arakawa, Y. Nakata, and T. Akiyama, Appl. Phys. Lett. **84**, 1820 (2004).

[29] D. L. Huffaker, G. Park, Z. Zou, O. B. Shchekin, and D. G. Deppe, Appl. Phys. Lett. **73**, 2564 (1998).

[30] H. S. Djie, B. S. Ooi, X.-M. Fang, Y. Wu, J. M. Fastenau, W. K. Liu, and M. Hopkinson, Opt. Lett. **32**, 44 (2007).

[31] H. Y. Liu, S. L. Liew, T. Badcock, D. J. Mowbray, M. S. Skolnick, S. K. Ray, T. L. Choi, K. M. Groom, B. Stevens, F. Hasbullah, C. Y. Jin, M. Hopkinson, and R. A. Hogg, Appl. Phys. Lett. **89**, 073113 (2006).

[32] George F. Koster, John O. Dimmock, Robert G. Wheeler, and Hermann Statz, *Properties of the Thirty-Two Point Groups* (MIT Press, Cambridge, MA, 1963).

[33] N. Liu, J. Tersoff, O. Baklenov, A. L. Holmes, Jr., and C. K. Shih, Phys. Rev. Lett. **84**, 334 (2000).

[34] U. Denker, M. Stoffel, and O. G. Schmidt, Phys. Rev. Lett. **90**, 196102 (2003).

[35] T. Walther, A. G. Cullis, D. J. Norris, and M. Hopkinson, Phys. Rev. Lett. **86**, 2381 (2001).

[36] See Supplemental Material at http://link.aps.org/supplemental/10.1103/PhysRevB.89.205312 for distribution of Δ, θ, details of theoretical method and experiments, as well as the results of all samples.

[37] See for example, M. L. Mehta, *Random Matrices* (Academic, San Diego, 1991).

[38] B. I. Shklovskii, B. Shapiro, B. R. Sears, P. Lambrianides, and H. B. Shore, Phys. Rev. B **47**, 11487 (1993).

[39] Notice that we have taken the polarization angle of both bright states into account to symmetrize the distribution function, thus the distribution of polarization angle is somewhat different from that reported by Plumhof [22].

[40] M. Abbarchi, C. A. Mastrandrea, T. Kuroda, T. Mano, K. Sakoda, N. Koguchi, S. Sanguinetti, A. Vinattieri, and M. Gurioli, Phys. Rev. B **78**, 125321 (2008).

[41] L.-W. Wang, J. Kim, and A. Zunger, Phys. Rev. B **59**, 5678 (1999).

[42] L.-W. Wang and A. Zunger, Phys. Rev. B **59**, 15806 (1999).

[43] A. J. Williamson, L.-W. Wang, and A. Zunger, Phys. Rev. B **62**, 12963 (2000).

[44] P. N. Keating, Phys. Rev. **145**, 637 (1966); R. M. Martin, Phys. Rev. B **1**, 4005 (1970).

[45] J. E. Bernard and A. Zunger, Appl. Phys. Lett. **65**, 165 (1994).

[46] A. Silverman, A. Zunger, R. Kalish, and J. Adler, J. Phys.: Condens. Matter **7**, 1167 (1995).

[47] L. Bellaiche, S. H. Wei, and A. Zunger, Phys. Rev. B **54**, 17568 (1996).

[48] P. Atkinson, E. Zallo, and O. G. Schmidt, J. Appl. Phys. **112**, 054303 (2012).

[49] A. Rastelli, S. Stufler, A. Schliwa, R. Songmuang, C. Manzano, G. Costantini, K. Kern, A. Zrenner, D. Bimberg, and O. G. Schmidt, Phys. Rev. Lett. **92**, 166104 (2004).

[50] Z. R. Wasilewski, S. Fafard, and J. P. McCaffrey, J. Cryst. Growth **201**, 1131 (1999).

[51] Catherine Tonin, Richard Hostein, Valia Voliotis, Roger Grousson, Aristide Lemaitre, and Anthony Martinez, Phys. Rev. B **85**, 155303 (2012).

[52] Y. Leger, L. Besombes, L. Maingault, and H. Mariette, Phys. Rev. B **76**, 045331 (2007).

[53] H. Huo, A. Rastelli, and O. G. Schmidt, Appl. Phys. Lett. **102**, 152105 (2013).

[54] R. Singh and G. Bester, Phys. Rev. Lett. **103**, 063601 (2009).

[55] A. Mohan, M. Felici, P. Gallo, B. Dwir, A. Rudra, J. Faist, and E. Kapon, Nat. Photonics **4**, 302 (2010).

[56] T. Kuroda, T. Mano, N. Ha, H. Nakajima, H. Kumano, B. Urbaszek, M. Jo, M. Abbarchi, Y. Sakuma, K. Sakoda, I. Suemune, X. Marie, and T. Amand, Phys. Rev. B **88**, 041306(R) (2013).

[57] J. Treu, C. Schneider, A. Huggenberger, T. Braun, S. Reitzenstein, S. Höfling, and M. Kamp, Appl. Phys. Lett. **101**, 022102 (2012).

[58] Gediminas Juska, Valeria Dimastrodonato, Lorenzo O. Mereni, Agnieszka Gocalinska, and Emanuele Pelucchi, Nat. Photonics **7**, 527 (2013).

[59] N. Le Thomas, E. Herz, O. Schöps, U. Woggon, and M. V. Artemyev, Phys. Rev. Lett. **94**, 016803 (2005).

[60] Qing Zhong Zhao, Peter A. Graf, Wesley B. Jones, Alberto Franceschetti, Jingbo Li, Lin-Wang, and Kwiseon Kim, Nano Lett. **7**, 3274 (2007).

[61] S. P. Ahrenkiel, O. I. Micic, A. Miedaner, C. J. Curtis, J. M. Nedeljkovic, and A. J. Nozik, Nano Lett. **3**, 833 (2003).

[62] Ming Gong, Jun-Wei Luo *et al.* (unpublished).

[63] K. Takehana, F. Pulizzi, Takehana. Patane, M. Henini, P. C. Main, L. Eaves, D. Granados, and J. M. Garcia, J. Cryst. Growth **251**, 155 (2003).

[64] J. C. Lina, P. W. Frya, R. A. Hogga, M. Hopkinsona, I. M. Rossb, A. G. Cullisb, R. S. Kolodkac, A. I. Tartakovskiic, and M. S. Skolnickc, Microelectron. J. **37**, 1505 (2006).

[65] M. Gendry, C. Monat, J. Brault, P. Regreny, G. Hollinger, B. Salem, G. Guillot, T. Benyattou, C. Bru-chevallier, G. Bremond, and O. Marty, J. Appl. Phys. **95**, 4761 (2004).

Supplementary materials for "Statistical Properties of Exciton Fine Structure Splittings and Polarization Angles in Quantum Dot Ensemble

Ming Gong[1,2],* B. Hofer[3], E. Zallo[3], R. Trotta[3,4],†

Jun-Wei Luo[5,6],‡ O. G. Schmidt[3], and Chuanwei Zhang[2]

[1]*Department of Physics, The Chinese University of Hong Kong, Shatin, New Territories, Hong Kong, China*

[2]*Department of Physics, The University of Texas at Dallas, Richardson, TX, 75080 USA*

[3]*Institute for Integrative Nanosciences, IFW Dresden, Helmholtzstr, 20, D-01069 Dresden, Germany*

[4]*Institute of Semiconductor and Solid State Physics, Johannes Kepler University Linz, Altenbergerstr. 69 A-4040 Linz, Austria*

[5]*State Key Laboratory of Superlattices and Microstructures, Institute of Semiconductors, Chinese Academy of Sciences, P.O. Box 912, Beijing 100083, China*

[6]*Synergetic Innovation Center of Quantum Information and Quantum Physics, University of Science and Technology of China, Hefei, Anhui 230026, China*

(Dated: April 16, 2014)

Abstract

This supplementary material contains the following six parts:

I. Distribution of FSS in QDE.

II. Distribution of Polarization Angles in QDE.

III. Details for the Atomistic Pseudopotential Calculations.

IV. Sample Details for Experimental grown QDEs E1 - E4.

V. Original Theoretical/Experimental Data

PACS numbers: 78.67.Hc, 42.50.-p, 73.21.La, 81.07.Ta

I: DISTRIBUTION OF FSS

The FSS reads as

$$\Delta = 2\sqrt{(\delta_0+\delta')^2+\kappa^2}. \tag{1}$$

Then the distribution of FSS reads as

$$\begin{aligned} P(\Delta) &= \int d\delta' d\kappa \delta(2\sqrt{(\delta_0+\delta')^2+\kappa^2}-\Delta)\frac{1}{\sqrt{2\pi}\sigma_{\delta'}}\frac{1}{\sqrt{2\pi}\sigma_\kappa}\exp(-\frac{\delta'^2}{2\sigma_{\delta'}^2}-\frac{\kappa^2}{2\sigma_\kappa^2}) \\ &= \int_0^{2\pi} d\phi \int_0^\infty dR R\delta(2R-\Delta)\frac{1}{2\pi\sigma_{\delta'}\sigma_\kappa}\exp(-\frac{(R\cos(\phi)-\delta_0)^2}{2\sigma_{\delta'}^2}-\frac{(R\sin(\phi))^2}{2\sigma_\kappa^2}) \\ &= \int_0^{2\pi} d\phi \frac{\Delta}{8\pi\sigma_{\delta'}\sigma_\kappa}\exp(-\frac{(\Delta\cos(\phi)-2\delta_0)^2}{8\sigma_{\delta'}^2}-\frac{(\Delta\sin(\phi))^2}{8\sigma_\kappa^2}) \\ &= \frac{\Delta}{8\pi\sigma_{\delta'}\sigma_\kappa}\exp(-\frac{\delta_0^2}{2\sigma_{\delta'}^2}-\frac{\Delta^2}{16\sigma_{\delta'}^2}-\frac{\Delta^2}{16\sigma_\kappa^2})J_1(\frac{\Delta^2}{16\sigma_\kappa^2}-\frac{\Delta^2}{16\sigma_{\delta'}^2},\frac{\delta_0\Delta}{2\sigma_{\delta'}^2}), \end{aligned} \tag{2}$$

where we have defined

$$J_1(a,b) = \int_0^{2\pi}\exp(-a\cos(2\phi)+b\cos(\phi))d\phi. \tag{3}$$

We can obtain Eq. 5 in the main text by setting $\delta_0 = 0$ in the above result, and Eq. 4 by setting $\delta_0 = 0$ and $\sigma_\kappa = \sigma_\delta$.

II: DISTRIBUTION OF POLARIZATION ANGLE

The polarization angle for the two bright states satisfies the following equation

$$\tan(\theta) = \frac{\delta \pm \sqrt{\delta^2+\kappa^2}}{\delta}. \tag{4}$$

If we define $\delta = R\cos(\phi)$, and $\kappa = R\sin(\phi)$, then we find

$$\begin{aligned} P_\pm(\theta) &= \int d\delta' d\kappa \delta(\theta-\text{atan}(\frac{(\delta_0+\delta')-\sqrt{(\delta_0+\delta')^2+\kappa^2}}{\kappa}))\frac{1}{\sqrt{2\pi}\sigma_{\delta'}}\frac{1}{\sqrt{2\pi}\sigma_\kappa}\exp(-\frac{\delta'^2}{2\sigma_{\delta'}^2}-\frac{\kappa^2}{2\sigma_\kappa^2}) \\ &= \int_0^\infty dR R\int_0^{2\pi} d\phi\delta(\frac{\phi}{2}-\theta)\frac{1}{2\pi\sigma_{\delta'}\sigma_\kappa}\exp(-\frac{(R\cos(\phi)-\delta_0)^2}{2\sigma_{\delta'}^2}-\frac{(R\sin(\phi))^2}{2\sigma_\kappa^2}) \\ &= \int_0^\infty dR R\frac{1}{\pi\sigma_{\delta'}\sigma_\kappa}\exp(-\frac{(R\cos(2\theta)-\delta_0)^2}{2\sigma_{\delta'}^2}-\frac{(R\sin(2\theta))^2}{2\sigma_\kappa^2}) \\ &= \frac{1}{\pi\sigma_{\delta'}\sigma_\kappa}\exp(-\frac{\delta_0^2}{2\sigma_{\delta'}^2})J_2(\frac{\cos(2\theta)^2}{2\sigma_{\delta'}^2}+\frac{\sin(2\theta)^2}{2\sigma_\kappa^2},\frac{\delta_0\cos(2\theta)}{\sigma_{\delta'}^2}), \end{aligned} \tag{5}$$

where

$$J_2(a,b) = \int_0^\infty dR R\exp(-aR^2+bR). \tag{6}$$

The measured distribution then reads as

$$P(\theta) = \frac{1}{2}(P_{-}(\theta) + P_{+}(\theta)). \tag{7}$$

We can obtain Eq. 6 in the main text by setting δ_0 in the above result.

III: DETAILS FOR THE ATOMISTIC THEORY

We employ the million-atom atomistic theory to confirm the theoretical predictions using $In_xGa_{1-x}As$/GaAs QDs. The alloyed QDs are embedded into a 60×60×60 eight-atom GaAs supercell. Due to the large lattice mismatch ($\sim 7\%$) between the dot material ($In_xGa_{1-x}As$) and the matrix (GaAs), we first have to relax the total strain energy to get the true equilibrium position $\{\mathbf{R}_{i,\alpha}\}$ with i the site index and α the atom type index. Here the total strain energy is modeled using valance force field model[1–3], which has been been successfully applied to various III-V group semiconductor systems[2–6, 8].

The single particle energy levels and the corresponding wavefunctions are obtained by solving the following Schrodinger equation

$$(-\frac{1}{2}\nabla^2 + V_{\rm ps}(\mathbf{r}))\psi_i(\mathbf{r}) = E_i\psi_i(\mathbf{r}) \tag{8}$$

where the pseudopotential $V_{\rm ps}(\mathbf{r}) = V_{\rm so} + \sum_{i,\alpha} v_\alpha(\mathbf{r} - \mathbf{R}_{i,\alpha})$ is the superposition of local screened atomic pseudopotentials. The first term contains the contribution of nonlocal spin-orbit coupling, and the second term contains contribution of all the atoms at equilibrium position. The pseudopotentials are fitted to physical important parameters such as the effective mass, the band gap width, unstrained band offsets, and hydrostatic and biaxial deformation potentials at the high symmetry points, e.g., Γ, K and L points in the first Brillouin zone. In this work, the pseudopotential parameters for InAs and GaAs are taken from Ref. 3. We see that the potential at site $\mathbf{r}$ contains the contribution of all sites in the whole lattice system, thus a small variation of the equilibrium position $\{\mathbf{R}_{i,\alpha}\}$ can lead to a small changes of the screened pseudopotential, which is the basic reason why our model has resolution of atomistic size. Thus for two QDs with the same morphology but different alloy configurations, their pseudopotentials are still different, hence their corresponding FSS and polarization angles may be fairly different. It is also exactly this reason that the V_1 term can be treated as random potentials from the view point of QDE.

The Schrodinger equation is solved by expanding the wavefunction as linear combination of bulk bands (LCBB) [3, 9, 10] basis, which reads as

$$\psi_i = \sum_{m,\mathbf{k},\lambda} c_{m,\mathbf{k},\lambda} \psi_{m,\mathbf{k},\lambda,\vec{\epsilon}} \tag{9}$$

where m is the band index, $\mathbf{k}$ is the wavevector of the material $\lambda =$ InAs, GaAs, that strained uniformly to strain $\vec{\epsilon}$. We use m =2, 3, 4 for the hole sector and $m = 5$ for the electron sector on a $6 \times 6 \times 16$ $\mathbf{k}$ mesh.

The exciton energies are calculated using the configuration interaction method[11], where the wavefunction of the exciton states are construted using the Slater determinants of all the confined electron and hole single particle states. The precision of the FSS can be smaller than 0.1 μeV in all our calculations. This method has been successfully applied to study the FSS in QDs, see Ref. [2, 8, 12–16].

IV: SAMPLE DETAILS FOR EXPERIMENTAL GROWN QDES E1 - E4

We consider three different types of QDEs in our experiments: the GaAs/AlGaAs QDEs (E1), the quantum well potential fluctuations (QWPFs) induced GaAs QDEs (E2, E3) and the In(Ga)As QDs (E4). We use two different samples containing GaAs/AlGaAs QDs grown via solid molecular beam epitaxy (MBE) on GaAs substrates. Both, excitons from the QDs and the confined states in the rough QW were studied. For the first sample (E1 and E2) a 99 nm-thick i-GaAs layer was grown on top of a 100 nm-thick $Al_{0.75}Ga_{0.25}As$ sacrificial layer. A low density ($n < 1 \times 10^8/\mathrm{cm}^2$) of nanoholes was created by droplet etching epitaxy[17] Then a bottom barrier layer of 7 nm $Al_{0.44}Ga_{0.56}As$ was deposited on top of the nanoholes followed by 3 nm GaAs and a 2 minutes interruption allowing GaAs to migrate towards the nanoholes. After this the formed QDs were capped with a 112 nm-thick $Al_{0.33}Ga_{0.67}As$ barrier layer and 20 nm-thick $Al_{0.44}Ga_{0.56}As$ layer. Finally, the sample was capped with a 19 nm-thick GaAs layer. For the second sample (E3) InAs QDs were grown on GaAs substrates. After 10 nm GaAs cap layer the $AsBr_3$ etching was used to convert the InAs QDs into nanoholes[18]. A 7 nm-thick $Al_{0.45}Ga_{0.55}As$ layer was grown on top of the nanoholes followed by a 2 nm layer of GaAs and 100 nm $Al_{0.35}Ga_{0.65}As$ barrier layer. Finally the sample was capped with a 20 nm-thick $Al_{0.45}Ga_{0.55}As$ cladding layer and a 10 nm GaAs layer. For the third sample (E4) self- assembled In(Ga)As/GaAs QDs grown by Stranski-Krastanov technique at 500°C

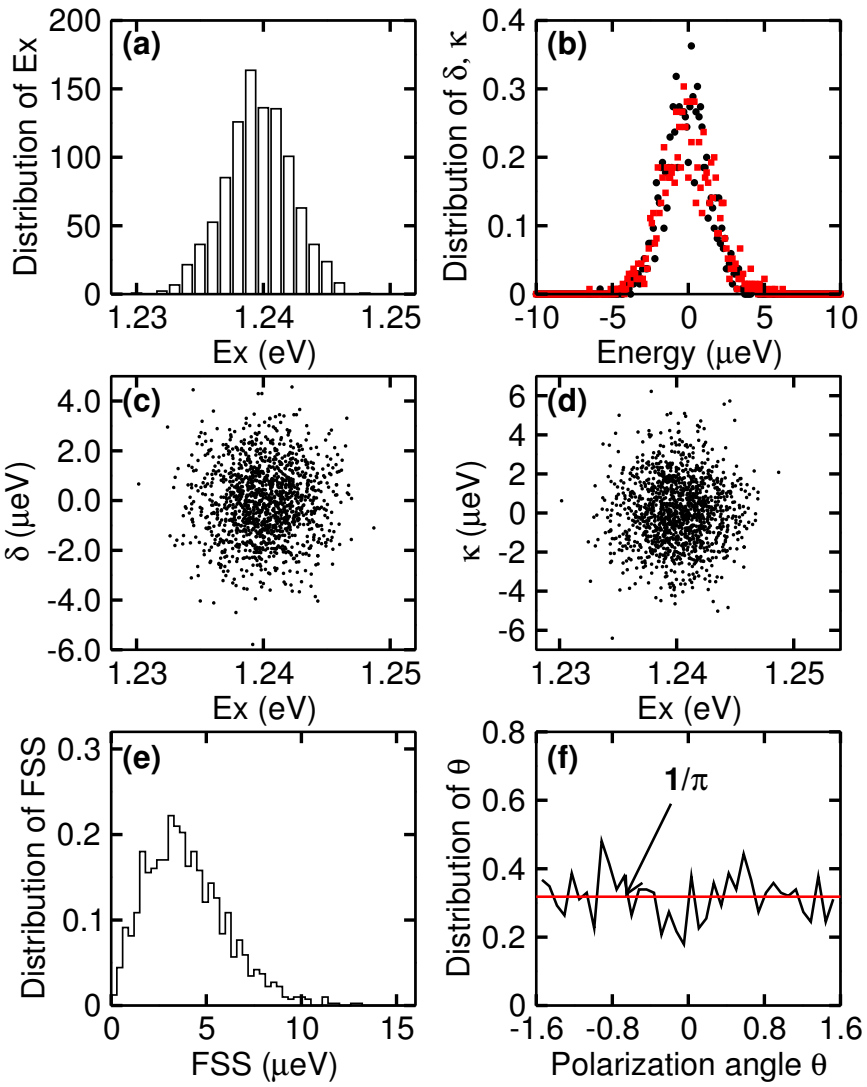

FIG. 1: Original data for QDE T1. (a) The distribution of exciton energy E_x. (b) The distribution of δ and κ. (c) and (d) show the energy dependence of δ and κ. (e) and (f) show the distribution of FSS and polarization angle .

were used. An indium flush step was introduced in order to control precisely the emission wavelength[19].

V: ORIGINAL THEORETICAL/EXPERIMENTAL DATA

* Email: skylark.gong@gmail.com

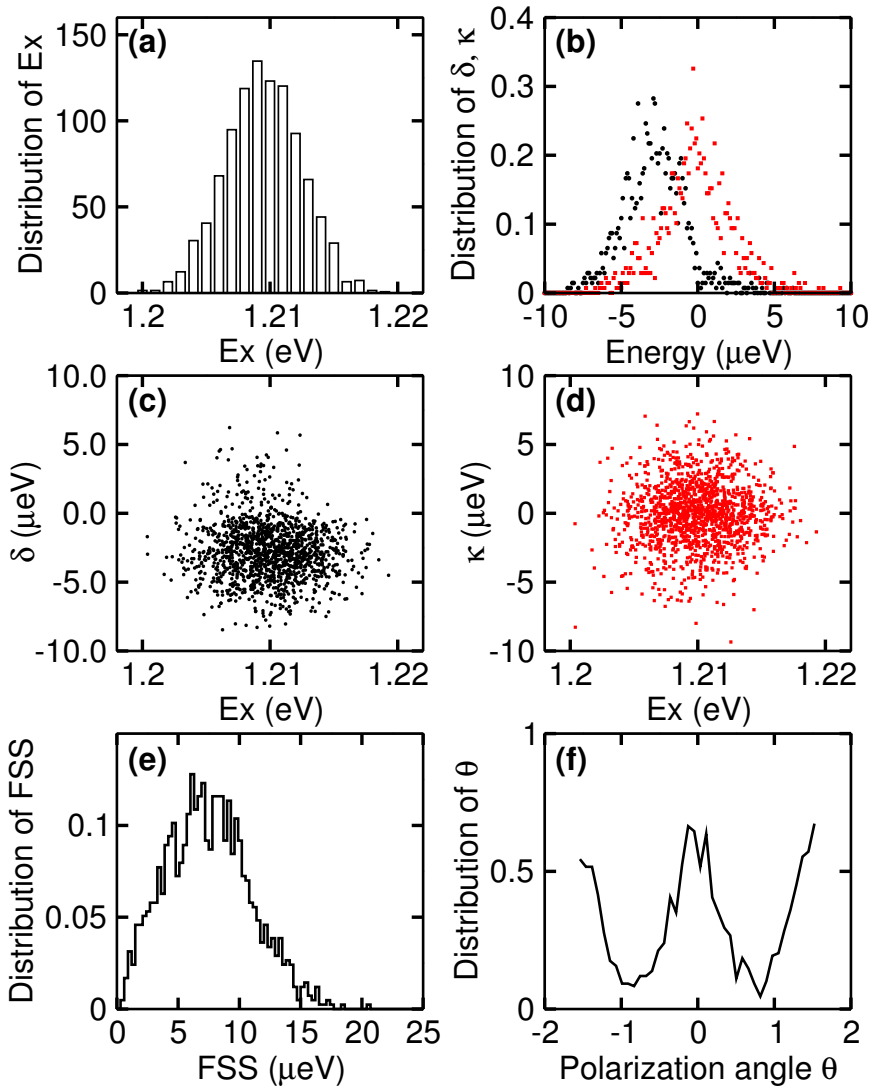

FIG. 2: Original data for QDE T2. (a) The distribution of exciton energy E_x. (b) The distribution of δ and κ. (c) and (d) show the energy dependence of δ and κ. (e) and (f) show the distribution of FSS and polarization angle .

† Email: rinaldo.trotta@jku.at

‡ Email: jwluo@semi.ac.cn

[1] P. N. Keating, Phys. Rev. **145**, 637 (1966); R. M. Martin, Phys. Rev. B **1**, 4005 (1970).

[2] Ming Gong, Kaimin Duan, Chuan-Feng Li, Rita Magri, Gustavo A. Narvaez, and Lixin He, Phys. Rev. B **77**, 045326 (2008).

[3] A. J. Williamson, L.-W. Wang, and A. Zunger, Phys. Rev. B **62**, 12963 (2000).

[4] J. E. Bernard and A. Zunger, Appl. Phys. Lett. **65**, 165 (1994).

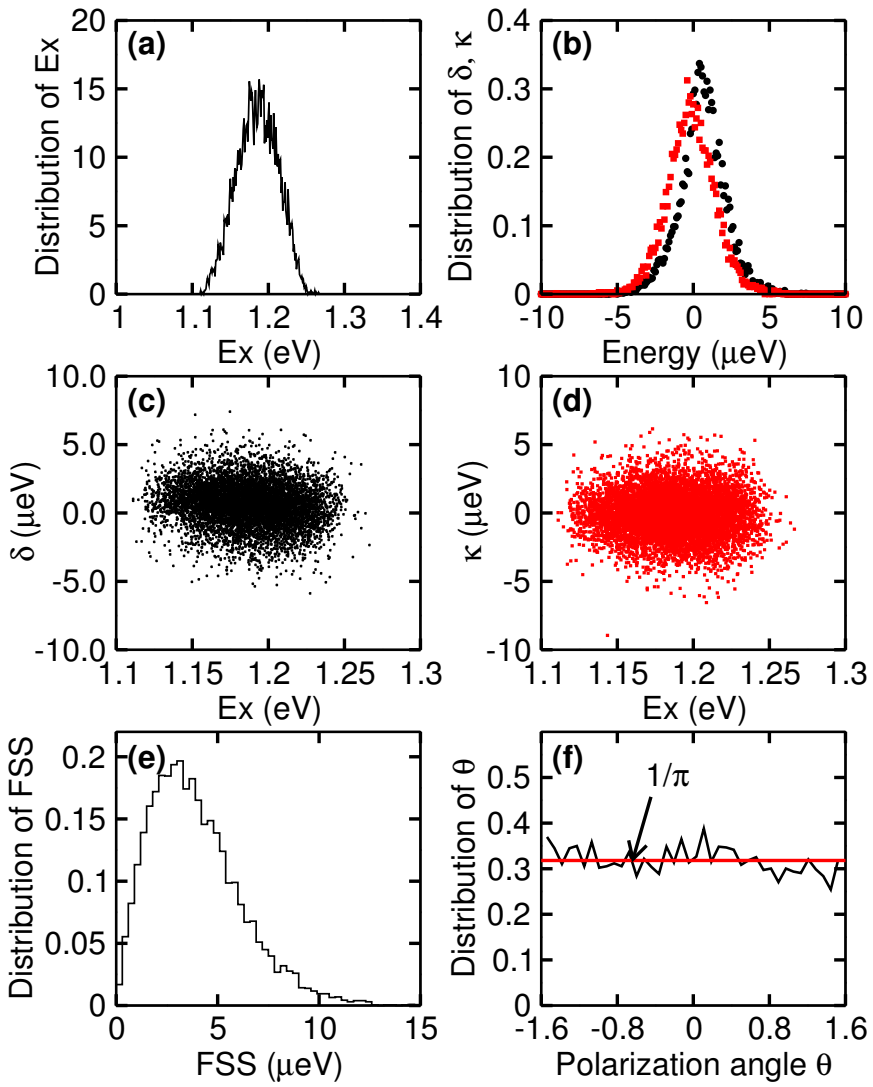

FIG. 3: Original data for QDE T3. (a) The distribution of exciton energy E_x. (b) The distribution of δ and κ. (c) and (d) show the energy dependence of δ and κ. (e) and (f) show the distribution of FSS and polarization angle .

[5] A. Silverman, A. Zunger, R. Kalish, and J. Adler, J. Phys.: Condens. Matter **7**, 1167 (1995).

[6] L. Bellaiche, S. H. Wei, and A. Zunger, Phys. Rev. B **54**, 17568 (1996).

[7] G. Bester and A. Zunger, Phys. Rev. B **71**, 045318 (2005).

[8] Jianping Wang, Ming Gong, Guang-can Guo and Lixin He, Appl. Phys. Lett. **101**, 063114 (2012).

[9] Lin-Wang Wang, Jeongnim Kim, and Alex Zunger, Phys. Rev. B **59**, 5678 (1999).

[10] Lin-Wang Wang and Alex Zunger, Phys. Rev. B **59**, 15806 (1999).

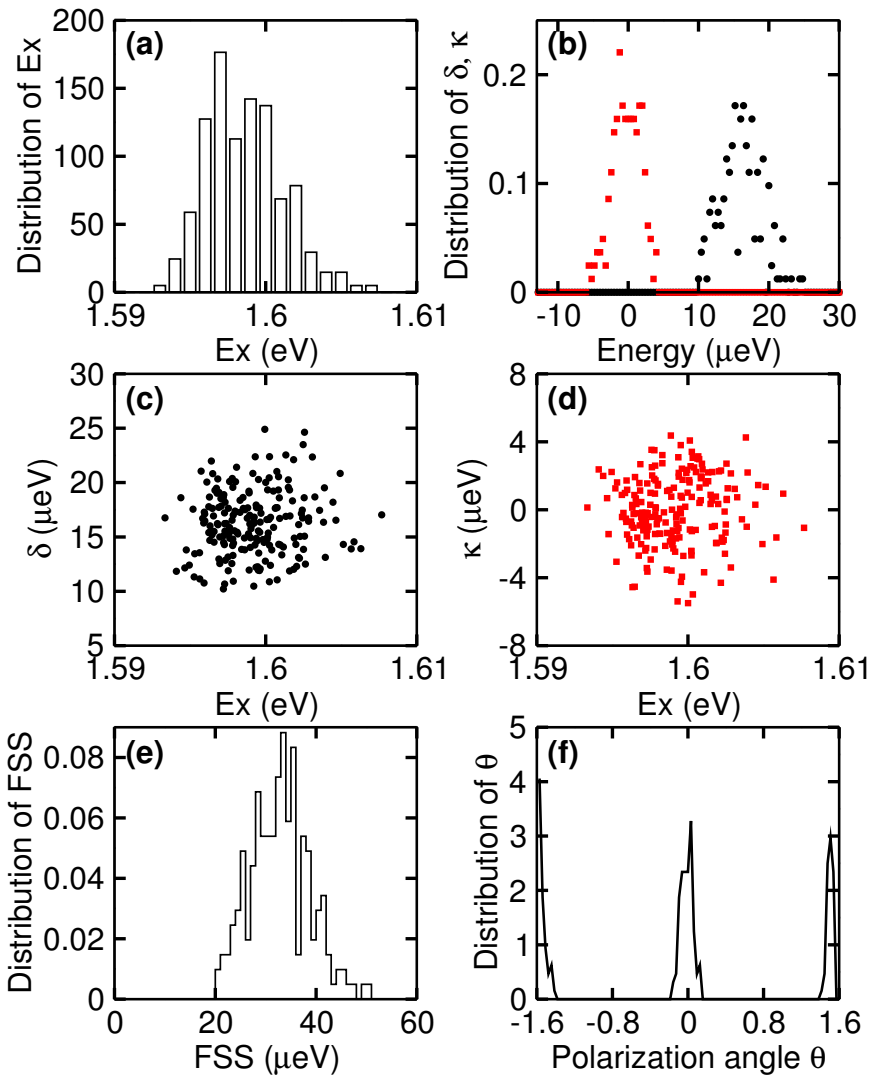

FIG. 4: Original data for QDE E1. (a) The distribution of exciton energy E_x. (b) The distribution of δ and κ. (c) and (d) show the energy dependence of δ and κ. (e) and (f) show the distribution of FSS and polarization angle.

[11] A. Franceschetti and A. Zunger, Europhys. Lett. **50**, 243 (2000).

[12] G. Bester, S. Nair, and A. Zunger, Phys. Rev. B **67**, 161306 (2003).

[13] G. Bester, and A. Zunger, Phys. Rev. B **71**, 045318 (2005).

[14] J. W. Luo, R. Singh, A. Zunger, and G. Bester, Phys. Rev. B **86**, 161302 (2012).

[15] R. Singh, and G. Bester, Phys. Rev. Lett. **104**, 196803 (2010).

[16] R. Singh, and G. Bester, Phys. Rev. Lett. **103**, 063601 (2009).

[17] P. Alonso-Gonzalez, J. Martn-Sanchez, Y. Gonzalez, B. Alen, D. Fuster, and L. Gonzalez,

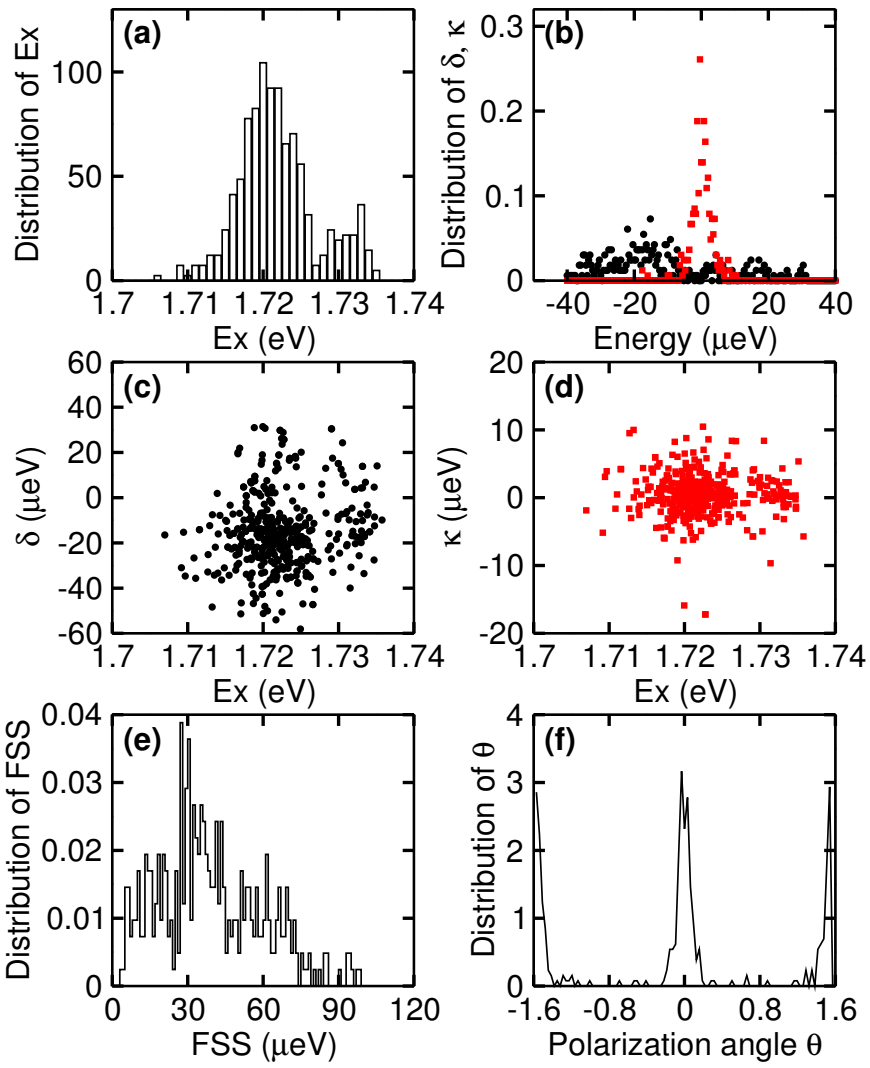

FIG. 5: Original data for QDE E2. (a) The distribution of exciton energy E_x. (b) The distribution of δ and κ. (c) and (d) show the energy dependence of δ and κ. (e) and (f) show the distribution of FSS and polarization angle.

Crystal Growth & Design, **9**, 2525 (2009).

[18] A. Rastelli, S. Stufler, A. Schliwa, R. Songmuang, C. Manzano, G. Costantini, K. Kern, A. Zrenner, D. Bimberg, and O. G. Schmidt, Phys. Rev. Lett. **92**, 166104 (2004).

[19] Z. R. Wasilewski, S. Fafard, and J. P. McCaffrey, Journal of Crystal Growth. **201**, 1131 (1999).

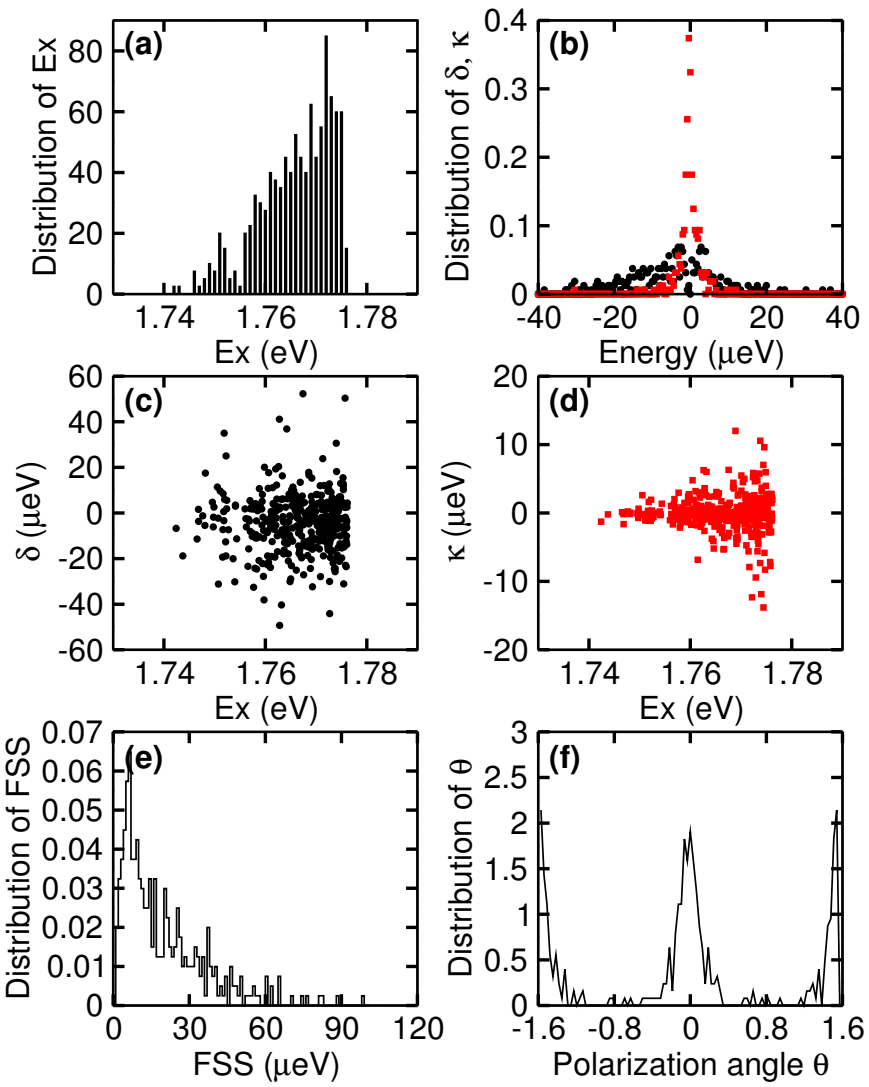

FIG. 6: Original data for QDE E3. (a) The distribution of exciton energy E_x. (b) The distribution of δ and κ. (c) and (d) show the energy dependence of δ and κ. (e) and (f) show the distribution of FSS and polarization angle.

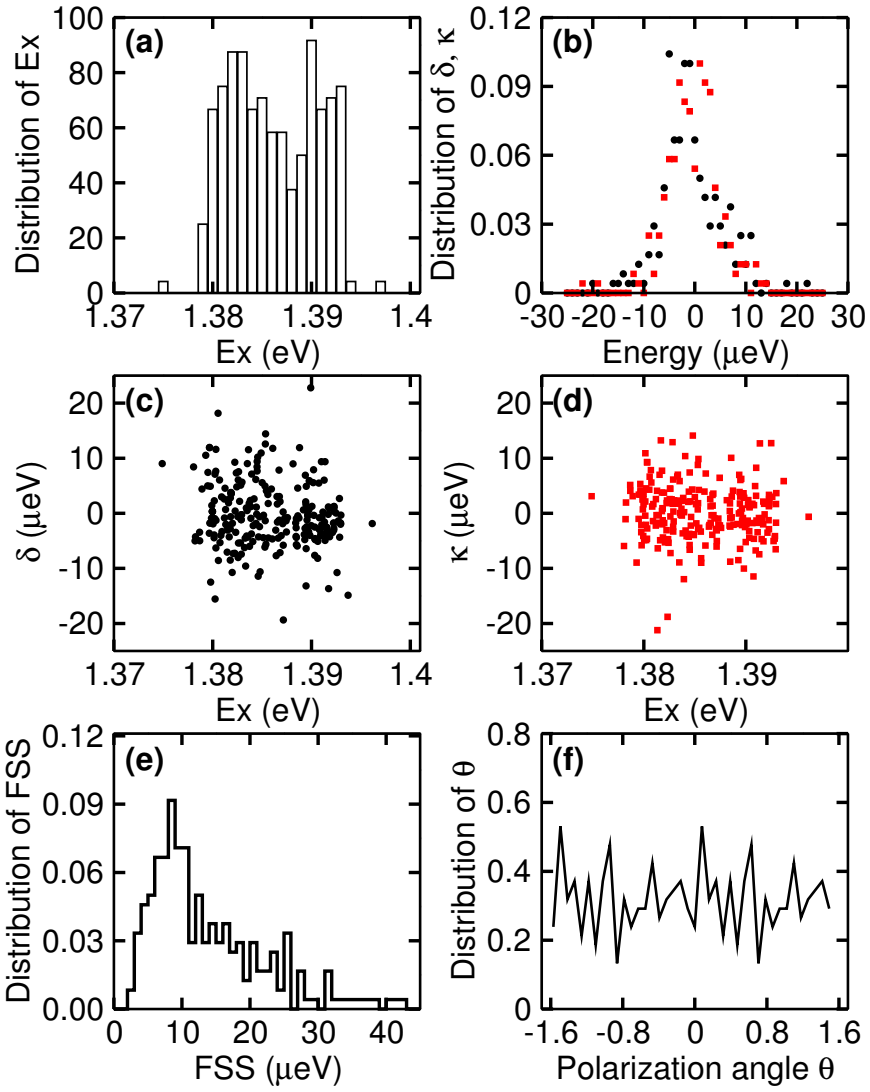

FIG. 7: Original data for QDE E4. (a) The distribution of exciton energy E_x. (b) The distribution of δ and κ. (c) and (d) show the energy dependence of δ and κ. (e) and (f) show the distribution of FSS and polarization angle .